Solar-driven semi-conductor photocatalytic water treatment (TiO2, g-C3N4, and TiO2+g-C3N4) of cyanotoxins: proof-of-concept study with microcystin-LR.

PESTANA, C.J., HUI, J., CAMACHO-MUÑOZ, D., EDWARDS, C., ROBERTSON, P.K.J., IRVINE, J.T.S. and LAWTON, L.A.

2022

Chemosphere 310 (2023) 136828

Contents lists available at ScienceDirect

Chemosphere

journal homepage: www.elsevier.com/locate/chemosphere

Solar-driven semi-conductor photocatalytic water treatment (TiO_2, g-C_3N_4, and TiO_2+g-C_3N_4) of cyanotoxins: Proof-of-concept study with microcystin-LR

Carlos J. Pestana [a,*,1], Jianing Hui [b,1], Dolores Camacho-Muñoz [a], Christine Edwards [a], Peter K.J. Robertson [c], John.T.S. Irvine [b], Linda A. Lawton [a]

[a] School of Pharmacy and Life Sciences, Robert Gordon University, Garthdee Road, Aberdeen, Scotland, AB10 7GJ, UK
[b] School of Chemistry, University of St Andrews, North Haugh, St Andrews, Scotland, KY16 9ST, UK
[c] School of Chemistry and Chemical Engineering, The Queen's University of Belfast, Stanmillis Road, Belfast, Northern Ireland, BT9 5AG, UK

HIGHLIGHTS

- Sunlight activated g-C_3N_4 & TiO_2+g-C_3N_4 removed MC-LR in less than 2 h.
- TiO_2+g-C_3N_4 removed MC-LR more rapidly than g-C_3N_4 alone under simulated sunlight.
- LC-MS confirmed similar MC-LR degradation pathways by all three catalysts.
- Facile coating method of TiO_2+g–C_3N_4–coating allows for ready scale-up of production.
- Rapid solar degradation of MC-LR by coated beads ideal for in-reservoir treatment.

GRAPHICAL ABSTRACT

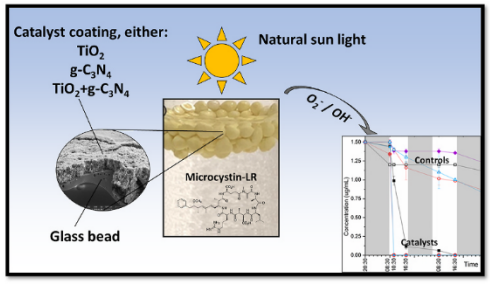

ARTICLE INFO

Handling Editor: Tsair-Fuh

Keywords:
In-reservoir treatment
Water treatment
Visible light photocatalysis
Graphitic-carbon nitride
Titanium dioxide

ABSTRACT

Cyanobacteria and their toxins are a threat to drinking water safety as increasingly cyanobacterial blooms (mass occurrences) occur in lakes and reservoirs all over the world. Photocatalytic removal of cyanotoxins by solar light active catalysts is a promising way to purify water at relatively low cost compared to modifying existing infrastructure. We have established a facile and low-cost method to obtain TiO_2 and g-C_3N_4 coated floating photocatalysts using recycled glass beads. g-C_3N_4 coated and TiO_2+g-C_3N_4 co-coated beads were able to completely remove microcystin-LR in artificial fresh water under both natural and simulated solar light irradiation without agitation in less than 2 h. TiO_2 coated beads achieved complete removal within 8 h of irradiation. TiO_2+g-C_3N_4 beads were more effective than g-C_3N_4 beads as demonstrated by the increase reaction rate with reaction constants, 0.0485 min^{-1} compared to 0.0264 min^{-1} respectively, with TiO_2 alone found to be considerably slower 0.0072 min^{-1}. g-C_3N_4 based photocatalysts showed a similar degradation pathway to TiO_2 based photocatalysts by attacking the C6–C7 double bond on the Adda side chain.

* Corresponding author.
E-mail address: c.pestana@rgu.ac.uk (C.J. Pestana).
[1] These authors contributed equally.

https://doi.org/10.1016/j.chemosphere.2022.136828
Received 24 March 2022; Received in revised form 5 October 2022; Accepted 7 October 2022
Available online 11 October 2022

The findings of this work demonstrate the potential for in-reservoir deployment of floating photocatalysts to achieve solar-driven photocatalytic destruction of cyanotoxins.

1. Introduction

Increasing temperatures and available nutrients lead to increased occurrence and severity of cyanobacterial mass events called blooms (Paerl and Huisman, 2008). Cyanobacterial blooms challenge water treatment with increased biomass (organic load) along with the potential for cyanotoxins and/or taste and odour compounds entering water treatment plants (WTPs) with the raw water. Cyanotoxins are harmful to humans (Humpage and Cunliffe, 2021) and are considered to be a risk to drinking water safety (WHO, 2020). The peptide hepatotoxins, microcystins (MCs) are the most commonly reported cyanotoxins across the globe and the World Health Organisation recommends a maximum allowable limit of combined MCs, of 1 μg L^{-1} in drinking water (WHO, 2020).

Therefore, there is an increasing requirement for water treatment utilities to have the capability to remove cyanobacteria and their toxins prior to them entering the drinking water treatment process. Conventional water treatment is often overwhelmed during bloom conditions and retro fitting existing WTP infrastructure is usually impractical and costly. Recently, in-reservoir treatment has become an attractive option for the removal of cyanobacteria and their toxic secondary metabolites. Chemical treatments like chlorine, chlorine dioxide and potassium permanganate application have been shown to be effective in the removal of some cyanobacteria, but can, upon cell lysis, introduce high concentrations of dissolved toxins into the raw water (Chow et al., 1999; Rodríguez et al., 2007a, 2007b). Hydrogen peroxide can decrease cyanobacterial biomass and remove subsequently liberated toxins (Matthijs et al., 2012; Santos et al., 2021), however, hydrogen peroxide breaks down rapidly (often within minutes) and treatment may be short lived.

Recent research has demonstrated that advanced oxidation processes (AOPs), particularly semiconductor photocatalysis, are an effective and environmentally acceptable means to remove cyanotoxins, via strongly oxidizing reactive oxygen species, such as hydroxyl radicals (Camacho-Muñoz et al., 2020; Gunaratne et al., 2020; Hui et al., 2021; Lawton et al., 1999; Pestana et al., 2020a, 2020b). Compared to other methods, photocatalysis does not require the use of additional chemicals during treatment and thus avoids potential pollution and the production of disinfection by-products. TiO_2 is a well-studied semiconductor and a broad range of compounds have been removed from water using this photocatalyst, ranging from dye degradation to cyanobacteria control (Liu et al., 2003; Pestana et al., 2020a, 2020b). Pestana et al. (2015) demonstrated that TiO_2 coated thin-walled, hollow glass spheres could decompose eleven different congeners of microcystins within several minutes under high-energy UV light irradiation (450 W). Furthermore, Pestana et al., 2020b and Menezes et al. (2021) demonstrated the successful removal of the cyanobacterium *Microcystis aeruginosa* and four of the MC congeners it produces using TiO_2 coated buoyant glass beads using UV-light emitting diodes.

Immobilization of a photocatalyst onto a buoyant matrix which could be deployed in a water body and activated by sunlight is highly desirable as it would allow widespread adoption of in-reservoir treatment (Wang et al., 2018; Xing et al., 2018). Wang et al., 2017 reported an F–Ce–TiO_2 with expanded perlite floating composites that removed 98.1% of *Microcystis aeruginosa* cells in 9 h under solar illumination. Gunaratne et al. (2020) demonstrated efficient destruction of microcystins by a UV-LED photoreactor pod containing TiO_2 immobilized floating recycled glass beads. Although TiO_2-based photocatalysts present excellent performance under UV light, in sunlight, activity is greatly reduced due to the small proportion of available UV light limiting practical application. Creating a heterojunction structure by combining TiO_2 with a visible light active photocatalyst is one method to solve this problem. g-C_3N_4, as a non-toxic organic semiconductor, has been explored for water treatment and gas purification (Cui et al., 2012; Nikokavoura and Trapalis, 2018; Song et al., 2018c). Song et al. (2018a) prepared a graphitic-C_3N_4 based photocatalyst and removed *M. aeruginosa* and the cyanotoxin MC-LR under artificial visible light irradiation.

While some studies have reported on heterojuctious photocatalyst for the removal of MC-LR, to the authors' knowledge, so far, no-one has reported on and compared the efficiency of immobilized TiO_2, g-C_3N_4 and the composite TIO_2+g-C_3N_4 onto a sustainable matrix (foamed beads made from recycled glass), prepared by a facile, readily scaled production method, and exposed to both natural and simulated solar irradiation. Previous reports have used high energy (up 1200 W m^{-2}) and/or artificial light sources (Song et al., 2018b, 2018c), powdered catalysts (Fan et al., 2019, 2022), or using an non-renewable matrix (perlite) (Song et al., 2018a).

In this work, we prepared catalyst coated (TiO_2, g-C_3N_4, g-C_3N_4+TiO_2) floating recycled glass beads via a facile calcination method that is readily scaled up to allow large scale production in a short period of time. The facility of the method stems from the avoidance of convoluted coating processes, the use of single pre-cursor compounds, and the lack of doping materials. The beads were irradiated with natural sunlight (Brazil) and simulated sunlight (laboratory) to investigate the destruction of the cyanotoxin MC-LR with the view to develop an application for in-reservoir treatment in the future.

2. Experimental

2.1. Materials and chemicals

Recycled glass beads produced from post-consumer glass (Diameter: 2–4 mm) were obtained from Dennert Poraver GmbH (Germany). P25 nanopowder (TiO_2, Anatase/Rutile: 85/15, 99.9%, 20 nm, Aeroxide) was purchased from Lawrence Industries Ltd, UK. Melamine (99%) was acquired from Sigma Aldrich and used as received. Isopropanol (2-propanol, ACS, 99.5%) was obtained from Alfa Aesar. Deionized (DI) water was used in all the experiments. MC-LR was obtained as per Edwards et al. (1996). Artificial freshwater was prepared according to Akkanen and Kukkonen (2003), in short $CaCl_2$ (58.8 mg L^{-1}), $MgSO_4$ (24.7 mg L^{-1}), $NaHCO_3$ (13.0 mg L^{-1}), and KCl (1.2 mg L^{-1}) were dissolved in ultrapure water (18.2 MΩ) and the pH adjusted to 7 with either HCl or NaOH (all chemicals were acquired from Fisher Scientific, UK). For the analytical determination of MC-LR, acetonitrile, and formic acid were acquired from Fisher Scientific and were of MS-gradient grade. Ultrapure water (18.2 MΩ) was provided by an Elga Purelab system (Veolia, UK).

2.2. Preparation of coated recycled glass beads

The preparation of g-C_3N_4 coated beads has been described in our previous report (Hui et al., 2021). In short, washed beads were mixed with 40% (w/w) melamine and calcined at 550 °C for 5 h in a covered crucible in air. The loading amount of g-C_3N_4 is about 10% (w/w) after removing unbound and soluble intermediate products.

TiO_2+g-C_3N_4 co-coated beads were prepared by coating a P25 aqueous suspension (0.1 g mL^{-1}) onto g-C_3N_4 coated beads and heating at 500 °C for 1 h TiO_2 coated beads with a catalyst loading around 10% (w/w) P25 nano-powder were also prepared by coating with a P25 aqueous suspension (0.1 g mL^{-1}), as described previously (Pestana et al., 2020b).

2.3. Characterization

Powder X-ray diffraction (XRD) was carried out on a PANalytical Empyrean X-ray diffractometer (Cu Kα1, reflection mode) to verify the phase. Ultraviolet–visible spectroscopy (UV–Vis) was collected on a JASCO-V650 spectrophotometer (Jasco Inc., USA). Fourier transform

infrared spectroscopy (FTIR) was carried out on a Shimadzu IRAffinity 1S IR Spectrometer. Brunauer-Emmett-Teller (BET) surface area of coated beads was measured on a Micrometrics TriStarII 3020 instrument. Surface morphologies and elemental distribution were characterized on a scanning electron microscope (SEM, FEI Scios DualBeam) and a transmission electron microscope (Titan Themis 200).

2.4. Photocatalytic destruction of MC-LR under sunlight

Photocatalytic degradation of MC-LR under solar irradiation was carried out in Fortaleza (3°43′6″S, 38°32′34″W), Brazil in October 2019. The photo-reactors were custom-built by placing 5 g coated beads (either g-C_3N_4+g-TiO_2, g-C_3N_4, or TiO_2), representing 0.15% (w/v) catalyst and providing a sufficient amount of beads to cover the surface of the reaction vessel in a single layer of beads, into a MC-LR solution in artificial fresh water (1.5 μg mL^{-1}; 350 mL) in a 500 mL polypropylene container. The concentration of 1.5 μg mL^{-1} MC-LR was selected to allow the observation of the removal of the cyanotoxin despite the fact that environmental concentrations are usually much lower (ng mL^{-1} range). To ensure the catalyst beads were submerged, a stainless-steel mesh (1.52 × 1.52 mm aperture size) was placed approximately 5 mm below the surface over the beads. Dark controls were prepared in an identical manner then coated with aluminium foil to exclude light. Light controls were also prepared in an identical manner without catalyst beads but exposed to sunshine. Each sample was prepared in triplicate. At the outset of the investigation all reactors were maintained in the dark for 12 h (dark adsorption). The reactors were then exposed to natural sunlight from sunrise to sunset, approximately 12 h per day with regular sampling. Samples (1 mL) were collected at T_0 dark adsorption, T_0 after 12 h dark adsorption; then at 2, 10, 13, 21, 24, 32, 35 and 44 h sunlight over 4 days allowing for day and night-time. To avoid an analyte concentration effect due to evaporation the water level in the reaction vessels was kept constant by the addition of appropriate amounts of ultrapure water. The pH was monitored by a pH meter (YSI, USA). A light meter (RS pro ILM201L) was used to monitor the luminous power of sunlight at the test site with readings converted by the Light Unit Converter App (Apogee Instruments, USA).

2.5. Photocatalytic destruction of MC-LR under simulated solar light

Degradation of MC-LR under simulated solar degradation was carried out in a SUNTEST XLS + Xenon arc weathering testing unit (ATLAS AMETEK Electronics Instrument Group, USA) operated with a daylight filter (cut off at <300 nm) operated at 60 W m^{-2} intensity. Aliquots of MC-LR (1.5 μg L^{-1}) in artificial freshwater (50 mL) were placed in beakers with 0.7 g of catalyst coated glass beads (either TiO_2, g-C_3N_4, or TiO_2+g-C_3N_4), representing 0.15% (w/v). Beads were kept submerged in the toxin solution by stainless-steel wire mesh disks (1.52 × 1.52 mm aperture size) placed approximately 5 mm below the surface of the solution. An initial sample (0.2 mL) was removed to determine the starting MC-LR concentration then beakers were placed in the dark for 12 h at 30 °C to allow dark adsorption and sampled again. The temperature was selected to mirror the conditions in Brazil. The beakers were exposed to simulated solar irradiation at 60 W m^{-2}, the irradiation chamber was temperature controlled to 30 °C, and samples were placed 320 mm from the light source. During simulated solar irradiation samples were removed at known intervals (1, 2, 4, 7, 10, 15, 30, 45, 60, 120, 240, 360, 480 min) and stored at 4 °C until analysed. As in the experiment in Brazil loss of experimental volume due to evaporation was replaced with ultrapure water. All experimental procedures were performed in triplicate. Control samples containing no beads (light control) and samples containing beads and kept in the dark (dark control) were prepared and sampled at the same time points.

2.6. Evaluation of coating stability by repeated photocatalytic dye degradation

A custom-made six-channel photoreactor was employed to evaluate the photocatalytic activity of coated beads after use using azo dye degradation (Fig. S1). An azo dye was chosen as target compound as a cost-effective alternative to microcystin-LR standards and for ease of concentration determination by UV/Vis spectroscopy. A Fe-doped metal halide lamp (250 W) was employed to provide UV–Visible light irradiation (>250 nm) for ease and rapidity of five repetition cycle. For rhodamine B (RhB) degradation, 400 mg coated beads (either TiO_2, g-C_3N_4, or TiO_2+g-C_3N_4; ~10% (w/w)) was added to 25 mL 6.5 mg mL^{-1} (0.02 mM) RhB aqueous solution. Solution (500 μL) was withdrawn at predetermined time intervals to analyse dye concentration on a V-550 spectrophotometer (λ = 555 nm; Jasco Inc., USA).

2.7. Analysis by UPLC-ESI-MS/MS and UPLC-ESI-QTOF-MS^E

MC-LR was analysed by ultra-high performance liquid chromatography coupled to tandem mass spectrometry (UPLC-MS/MS) using a targeted approach for quantification and untargeted approach (UPLC-ESI-QTOF-MS^E) for the identification of degradation products. Quantification of MC-LR was performed on a Waters Acquity UPLC system (Waters, UK) coupled to a triple quadrupole mass spectrometer (QqQ, Xevo TQ-XS, Waters, UK) with an electrospray ionization source (ESI) operated in positive ion mode (UPLC-ESI-MS/MS). Chromatography separation was achieved using a Waters Acquity UPLC BEH C18 column (50 × 2.1 mm, 1.7 μm; Waters, UK) held at 60 °C and a mobile phase gradient consisting of water and acetonitrile modified with 0.025% formic acid at 0.6 mL min^{-1} as described previously (Turner et al., 2018). Samples were maintained at 10 °C and the injection volume was 5 μL. The Xevo TQ-XS tune parameters were as follows (Turner et al., 2018): capillary voltage 1.0 kV, source temperature 150 °C, desolvation temperature 600 °C, desolvation gas flow 600 L h^{-1} (Nitrogen) and collision gas flow 0.15 mL min^{-1} (Argon). Data was acquired in the multiple reaction monitoring (MRM) mode (m/z 995.6 > 135.2, cone 60 V, collision energy 76 eV and m/z 995.6 > 107.3, cone 60 V, collision energy 74 eV). Quantification was conducted using external calibration with MC-LR standard.

Identification of MC-LR degradation products was performed on a Waters Acquity UPLC system (Waters, UK) coupled to a quadrupole time-of-flight mass spectrometer (QToF, Xevo G2-XS, Waters, UK) with an ESI operated in positive ion mode (UPLC-ESI-QTOF-MS^E). Chromatographic separation was carried out on a Waters Acquity UPLC BEH C18 column (100 × 2.1 mm, 1.7 μm; Waters, UK) held at 40 °C and a mobile phase gradient consisting of water (A) and acetonitrile (B) both modified with 0.1% formic acid at 0.3 mL min^{-1} as follows: 0 min–20% B; 6 min–70% B; 6.5 min–100% B; 7.5 min–100% B; 8 min–20% B; 10 min–20% B. Samples were kept at 5 °C and 5 μL was injected into the UPLC-ESI-QTOF-MS^E. The Xevo G2-XS tune parameters were as follows: capillary voltage 3.0 kV, cone voltage 20 V, source temperature 140 °C, desolvation temperature 600 °C, cone gas flow 100 L h^{-1} (Nitrogen), desolvation gas flow 1000 L h^{-1} (Nitrogen). Sodium formate was used as calibration solution over m/z 50–2000 and leucine enkephalin (m/z 556.2771) infused at 20 μL min^{-1} was used to correct for mass drifts. Data was acquired in centroid mode and two functions using low collision energy (6 V) and high collision energy (ramp 20–50 V) were acquired in the MSE mode. MassLynx v 4.2 software (Waters, UK) was used to acquire and process data.

3. Results and discussion

3.1. Photocatalytic destruction of MC-LR under natural and simulated sunlight

Under natural sunlight, static floating g-C_3N_4 beads and TiO_2+g-

C_3N_4 beads demonstrated very rapid (2 h at 159 μmol m^{-2} s^{-1}; 80.43 W m^{-2}) elimination of MC-LR (1.5 μg mL^{-1}). In comparison, under the same conditions the TiO_2 coated beads took 19 h illumination to achieve total MC-LR removal (Fig. 1). The destruction of MC-LR under solar illumination with TiO_2 coated beads is promising as the nano-powder (P25) used to coat the beads (Anatase/Rutile) absorbs UV light (≤390 nm) which typically represents around 5% of the total solar spectrum (Porfirio et al., 2012). While TiO_2+UV has been demonstrated to be an efficient way to decompose MC-LR via hydroxyl radicals generated on the photocatalyst surface (Lawton et al., 2003; Liu et al., 2003), low light utilization rates clearly limit the performance under natural sunlight. However, for non-time-critical applications (e.g. waste stabilization ponds) unmodified TiO_2 under solar irradiation could be a viable technology considering the low cost of the raw materials, ease of manufacture and scale up. Using either g-C_3N_4 beads and TiO_2+g-C_3N_4 beads greatly enhance degradation of MC-LR in sunlight with an almost 10-fold reduction in the treatment time which can be explained by the activation of the carbon nitride over an extended wavelength (≤460 nm), greatly increasing the useful energy available for photocatalytic treatment.

Dark adsorption onto the catalyst prior to illumination was relatively low, with the highest recorded for the TiO_2 (~20%) which is in keeping with our previous findings (Pestana et al., 2015, 2020a). Some loss of MC-LR was observed in the treatment with sunlight alone, where there was around a 7% decrease by 21 h of sunlight which increased to a loss of 27% at the end of the exposure time (44 h). It is not clear if all of this degradation is due to the natural actions of sunlight or other factors such as biodegradation as the reactors were open to the environment (León et al., 2019). Somewhat more degradation was observed in the dark control treatments containing g-C_3N_4, this was limited to around 7% in the first 2 h, however the loss reached 60% by the end of the study. It was also noted that the pH in the presence of the g-C_3N_4 increased to 9.5 (possibly due the intermediate products heptazine and poly(triazine imide) during g-C_3N_4 formation) which, combined with the elevated temperature (Fig. S2) and possible actions of microbes could account for this decline. Another possible cause of degradation in the controls could be due to short periods of illumination (~5 min) during sampling. Regardless, the time when the photocatalytic degradation occurs is much earlier (in the first day or so), hence this has little influence on the overall finding. Rapid degradation under solar irradiation was not anticipated, hence the sampling points were selected with longer time intervals. To understand the photocatalytic degradation process of MC-LR during the initial irradiation, a laboratory experiment was performed with simulated sunlight in an Atlas sunlight tester with a daylight filter (cutting off light below 300 nm) to simulate natural daylight in the laboratory. Simulated sunlight with a light intensity of 60 W m^{-2} (according to the manufacturer: equivalent to midday summer sun in Miami, Florida, similar to the study in Fortaleza, Brazil) was employed to elucidate degradation kinetics and transformation pathways.

Findings using the simulated sunlight source were comparable to those obtained for natural sunlight (Fig. 2): g-C_3N_4 beads and TiO_2+g-C_3N_4 beads performance was markedly better than TiO_2 beads with all MC-LR removed within 2 h, while the TiO_2 beads destroyed around 50% of the toxin after 2 h with complete removal achieved by 8 h (Fig. 2). TiO_2+g-C_3N_4 beads were more effective for the photocatalytic decomposition of MC-LR than g-C_3N_4 alone as demonstrated by the increased reaction rate with reaction constants of 0.0485 min^{-1} compared to 0.0264 min^{-1} respectively. TiO_2 alone was found to be considerably slower at 0.0072 min^{-1}.

Here, C_0 and C_t is the concentration at time 0 and t, k is the reaction constant. All three catalysts fit well to the pseudo-first-order kinetics (Fig. 3). TiO_2-decorated g-C_3N_4 clearly showed enhanced activity under simulated solar light, almost doubling the reaction constant (0.0485 min^{-1} compared to 0.0264 min^{-1}). This was probably because TiO_2 and g-C_3N_4 form a heterojunction structure which benefits electron transfer and thus suppresses the electron-hole recombination (Li et al., 2017; Ma et al., 2016).

The dark control samples showed little evidence of decomposition of the toxin, confirming that other factors would have influence the exposure in the natural environment (Fig. 1.). Light control samples without catalyst showed a 23% reduction of MC-LR after 8 h irradiation. These results concurred with the natural solar irradiation test, with a MC-LR reduction of 27%. Dark adsorption, which has been well documented for MC-LR in the presence of TiO_2 (Lawton et al., 2003; Pestana et al., 2015, 2020a), was between 7–12% (Fig. S3) for all catalysts. The mass of the photocatalytic beads remained unchanged following irradiation (Fig. S4) confirming stability of coated beads during treatment.

The photo-destruction of MC-LR has similar mechanism as photodegradation of other organic pollutants, with reactive oxygen species

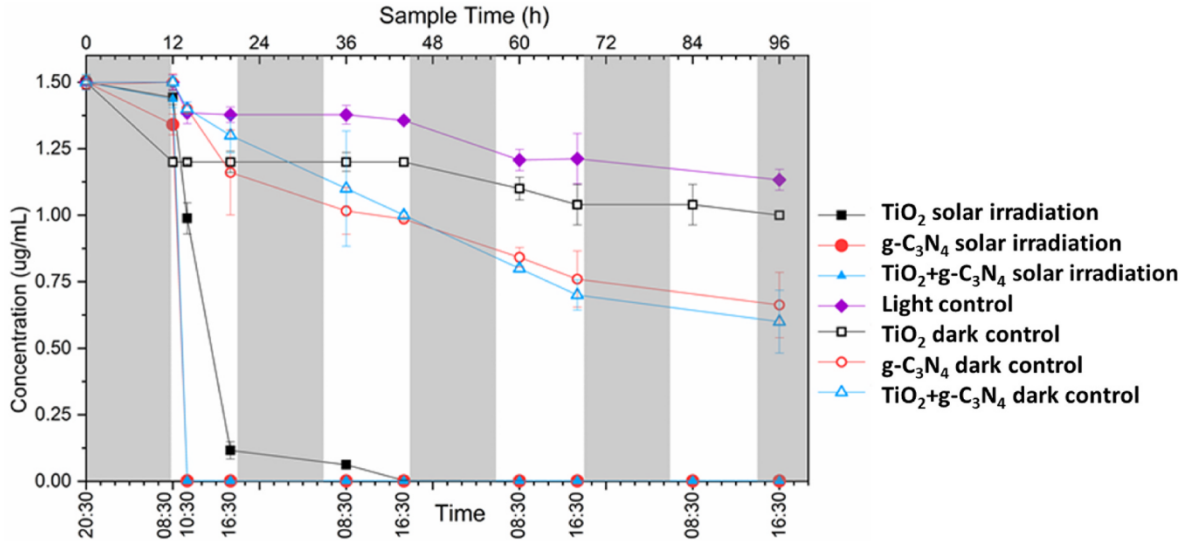

Fig. 1. Photocatalytic destruction of MC-LR under natural sunlight irradiation (159 μmol m^{-2} s^{-1}; 80.43 W m^{-2}, Brazil, October 2019) by floating, catalyst coated (g-C_3N_4, TiO_2 and TiO_2+g-C_3N_4) glass beads made from recycled glass. Initial MC-LR concentration was 1.5 μg mL^{-1} (n = 3, Error = 1SD). Grey area indicates the hours of darkness. Note: data series for g-C_3N_4 (red circle) and TiO_2+g-C_3N_4 (light blue triangles) are superimposed after the 12 h sampling time (08:30 on day 1). (For interpretation of the references to colour in this figure legend, the reader is referred to the Web version of this article.)

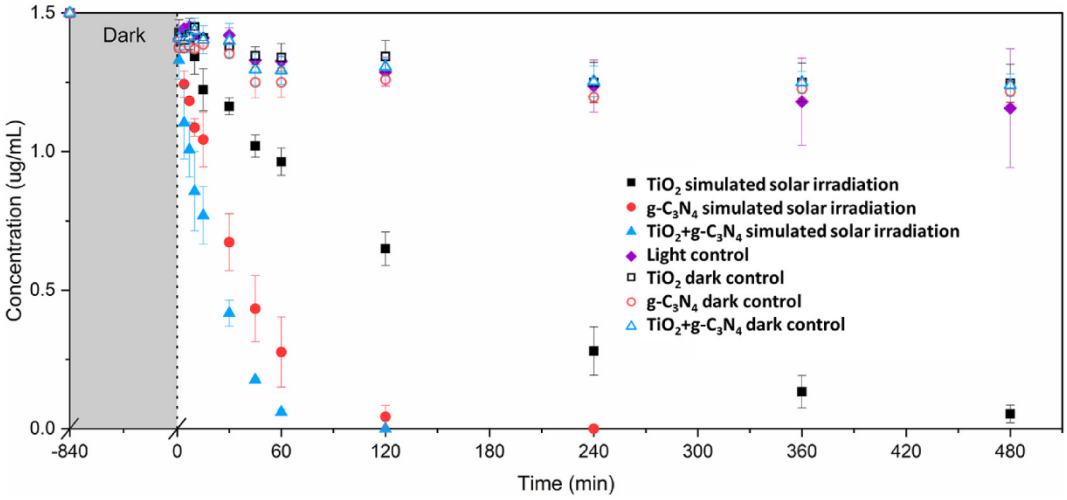

Fig. 2. Photocatalytic destruction of MC-LR under simulated sunlight irradiation in the presence of catalyst coated recycled glass beads (g-C_3N_4, TiO_2 and TiO_2+g-C_3N_4). Initial toxin concentration is 1.5 μg mL-1. (n = 3, Error = 1SD). The efficiency of MC-LR photo-destruction was evaluated by the pseudo-first-order model.

$$Ln(C_t / C_0) = kt \quad (1)$$

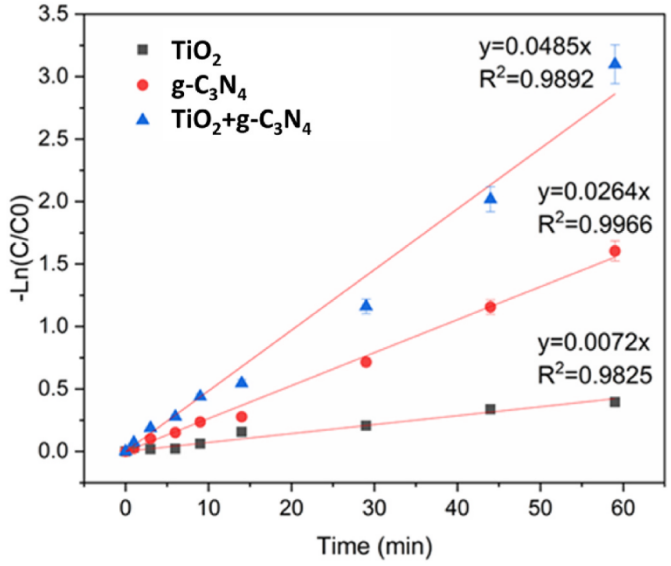

Fig. 3. Pseudo-first-order kinetics of MC-LR degradation under simulated sunlight.

(ROS) attacking the weaker bonds in organic molecules (Su et al., 2013). The attack sites in MC-LR such as double bonds of carbon in the Adda side chain and amino acids in the cyclic structure are highlighted in Fig. S5 (He et al., 2020). Since g-C_3N_4 has different band position to TiO_2, it is more likely to generate super oxide radical rather than hydroxyl radical in aqueous photocatalysis reactions (Hui et al., 2021; Kang et al., 2015). UPLC-ESI-QTOF-MS^E was used to compare the degradation intermediates observed for the different coatings (product ions Table. S1). Based on the first attack position within the MC-LR structure, different possible degradation pathways of MC-LR were proposed (He et al., 2020). When the attack occurred on the benzene ring and methoxy group of the Adda chain first (m/z values highlighted in yellow in Table. S1), an ion with m/z of 1011.6 was present in all three samples, which indicates that hydroxylation at the aromatic ring occurred. A further hydroxylation product (m/z = 1027.6) was only found in g-C_3N_4 containing samples (Andersen et al., 2014). A small Adda chain molecule with m/z of 289.2 was exclusively found in the sample with TiO_2 coated beads. As the hydroxyl radicals, generated by TiO_2, have a higher oxidizing potential compared to the other ROS species produced by g-C_3N_4, it is possible that TiO_2 is more efficient in the mineralization process of MC-LR than g-C_3N_4, leading to the presence of smaller transformation products.

The double carbon bonds on the Adda chain are also easy to be attacked by ROS (C4–C5 and C6–C7). When following the degradation pathway at a C4–C5 double bond break, only some hydroxylation intermediates were detected e.g. one hydroxylation addition (m/z = 1011.5) and double carbon bond hydroxylation (m/z = 1029.6). Another product with a m/z of 1025.5 may come from the conversion of a methoxy group to aldehyde (Fotiou et al., 2013). None of these samples displayed small molecule products following this degradation pathway. Based on the detected products, it is more likely that degradation follows a pathway that starts with an initial attack on the C6–C7 double bond. As highlighted in red in Table S1, ions with m/z = 1029.5 and 1045.5 are products of C6–C7 double bond hydroxylation and further benzene ring hydroxylation (Nawaz et al., 2018). The C6–C7 cleavage resulted in a small ion with m/z of 835.4. The ion with m/z = 745.4 could be a product of further amino acid oxidation in the Arg and Mdha groups. Wang et al. (2018) suggested gradual decarboxylation happened at Arg, Glu and MeAsp, and eventually formed an intermediate with m/z = 525.3. Further decarboxylation and deamination produced a smaller ion with m/z = 481.3 (Wang et al.,2017b, 2018). These intermediate products were found in all tested solutions using TiO_2 beads, g-C_3N_4 beads and TiO_2+g-C_3N_4 beads, which illustrated comparable degradation and mineralization effects of g-C_3N_4 and TiO_2.

The beads in the current study were produced with a facile coating process requiring a single pre-cursor compound in comparison to production methods that have been reported to date, which are convoluted, multi-step processes that require harmful chemicals, noble metals, and do not, readily, lend themselves to scaled up production for the quantities need needed for in-reservoir treatment. With the proposed facile coating method, the rate limiting step to large-scale production is the capacity of the muffle furnace. This, however, is readily overcome in an industrial setting, potentially allowing for the production of kilograms of coated beads at a time.

3.2. Characterization of TiO_2+g-C_3N_4 co-coated beads

The TiO_2+g-C_3N_4 co-coated beads demonstrated the fastest degradation of MC-LR. As this represents a novel coating, detailed characterization was carried out with comparison to g-C_3N_4 and TiO_2 coated beads. The TiO_2 (P25) loading amount is around 10% (w/w) after repeating the wet coating of P25 nano-powder. XRD (Fig. 4(a)) indicated a strong characteristic peak of the anatase phase at 25.2° accompanied by several weak peaks at a high angle. A weak, but noticeable, rutile peak was found at 27.5° which indicated a mixed phase of anatase with rutile consistent with P25. The heat treatment during the TiO_2 coating did not appear to cause crystal phase change. One characteristic peak at 26° was believed to result from the recycled glass beads which was observed in all three samples though the main structure of these beads was amorphous. It was difficult to confirm the crystal phase in the beads since there were only a few peaks observed from the secondary phases present in the waste-glass beads. Elemental quantification of the pristine beads is presented in Table S2. In TiO_2+g-C_3N_4 co-coated beads, a weak peak corresponding to the anatase phase was confirmed, as well as the main broad reflection peak (002) of graphitic-C_3N_4 phase at 27.5°. The intensity of g-C_3N_4(002) in co-coated beads was lower than that observed for the g-C_3N_4 coated materials. This was probably due to thermal decomposition during the latter's TiO_2 coating, which was coincident to the weight loss of g-C_3N_4 after TiO_2 coating. The g-C_3N_4 catalyst loading after a single coating was around 12% (w/w), which was verified by TGA in our recently published paper (Hui et al., 2021). On the other hand, the resulting TiO_2+g-C_3N_4 co-coated beads showed a similar 10% (w/w) catalyst loading, which means about 2% (w/w) of g-C_3N_4 loss after 1 h calcination at 500 °C in air.

The chemical structures of the coated recycled glass beads were examined using FTIR spectroscopy. The TiO_2+g-C_3N_4 co-coated beads displayed similar characteristic bands compared to g-C_3N_4 coated beads (Fig. 4(b)). The two wide and intense bands centred at 1000 cm^{-1} and 460 cm^{-1} are assigned to the internal vibrations in SiO_4 tetrahedra of the beads (Criado et al., 2007). The weak but sharp band at 810 cm^{-1} is from the tri-a-triazine breathing mode and the group bands at 1637, 1568, 1408, 1319 and 1242 cm^{-1} are associated with the vibration and stretching of C–N heterocycles. The broad weak band at around 3178 cm^{-1} is attributed to the N–H and O–H stretching vibration modes, which indicates the existence of free amino groups and hydroxyl species (Zhang et al., 2009).

The beads used in this work were 2–4 mm in diameter and had a relatively smooth surface. The surface area of the uncoated beads was 0.35 m^2/g. After coating with the same amount of TiO_2 and g-C_3N_4, the surface area increased to 2.63 and 2.33 m^2/g, respectively. The further coating of P25 nano-powder on g-C_3N_4 coated beads showed almost no change in the surface area (Fig. 4(c)).

The light absorption properties of the coated beads were studied by UV–Vis. TiO_2 coated beads exhibited a maximum absorption at 385 nm, while TiO_2+g-C_3N_4 coated beads had almost the same absorbance spectrum as g-C_3N_4 coated beads, with a maximum light absorption at 460 nm (Fig. 4(d)) as observed previously (Hui et al., 2021). This illustrated that both g-C_3N_4 and TiO_2+g-C_3N_4 coated beads can theoretically utilize a larger fraction of solar light compared to TiO_2 coated beads. The physical characteristics of the three different coated beads are summarised in Table 1.

The surface morphology of coated beads was examined using SEM, (Fig. 5(a-c)). The TiO_2-coated bead surface was covered by a fine P25

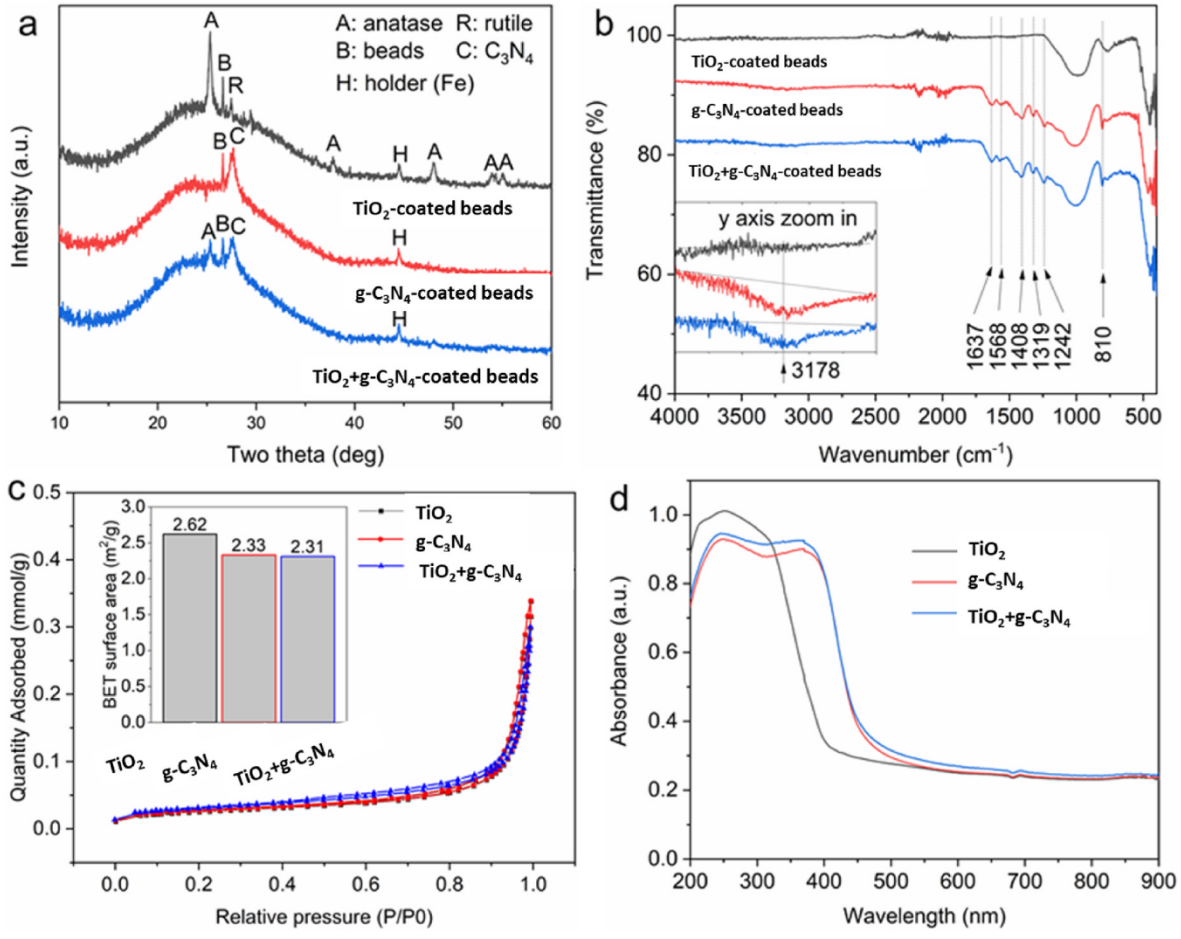

Fig. 4. Characterization of TiO_2; g-C_3N_4 and TiO_2+g-C_3N_4 coated recycled glass beads: (a) XRD; (b) FTIR; (c) N_2 adsorption-desorption isotherms; (d) UV–vis DRS.

Table 1
Physical information of TiO_2; g-C_3N_4 and TiO_2+g-C_3N_4 beads.

Sample	Diameter (mm)	Catalyst loading (w/w%)	BET surface area (m^2/g)	Bandgap (eV)
TiO_2	2–4	10	2.63	3.2
g-C_3N_4	2–4	10	2.33	2.7
TiO_2+g-C_3N_4	2–4	10	2.31	2.7

nano-powder. The size of the TiO_2 particles was between 20 and 30 nm, which is more obvious in TEM (Fig. S6). The morphology of g–C_3N_4–coated bead surface appeared to be porous but less uniform, displaying various textures. Some parts of the photocatalytic coating formed sheets while in other parts of the layer the sheets were curled to form hollow ball-like structures. This was more noticeable when scratching the surface material onto a TEM grid (Fig. S7). TiO_2+g-C_3N_4 beads displayed a mixed texture with fine TiO_2 nano-powder deposited on a porous g-C_3N_4 backbone. EDS results in Fig. 5(d) verified the elements on the three coated bead samples, with C, N and Ti detected on the surface of TiO_2+g-C_3N_4 beads. The recycled glass beads were found to contain Si, Ca and other metal elements such as Na, Mg, Al, (Table S2).

The microstructure of the coated active material was also investigated using TEM (Fig. S8 shows a graphitic-C_3N_4 sheet decorated with TiO_2 nano-particles). The TiO_2+g-C_3N_4 scrappings were ground with ethanol and dropped onto the TEM grid, and the g-C_3N_4 sheet spread out across the carbon grid. Under the TEM the material looked very thin

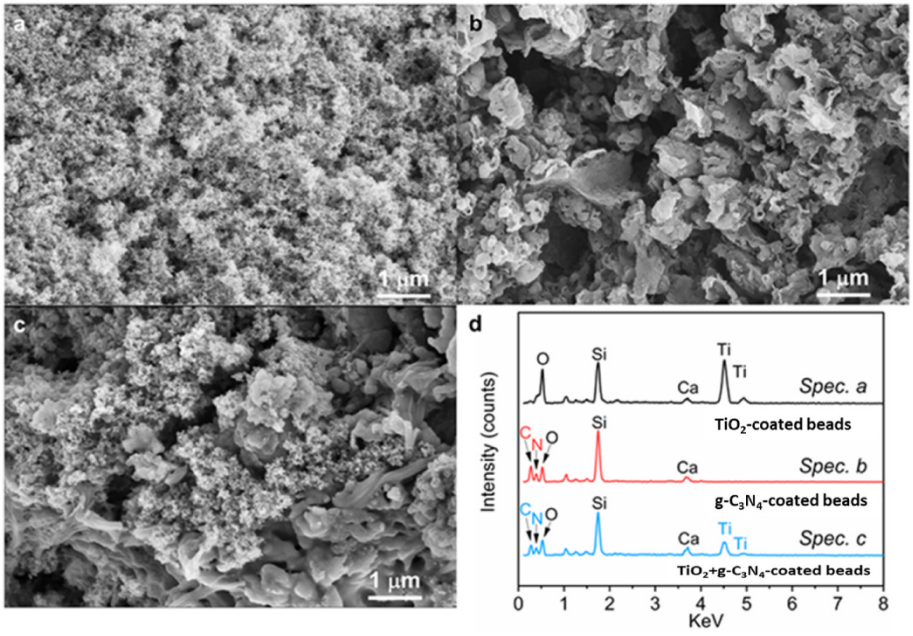

Fig. 5. SEM images of TiO_2 (a); g-C_3N_4 (b); TiO_2+g-C_3N_4 co-coated recycled glass beads (c); and EDS spectra of these three samples (d).

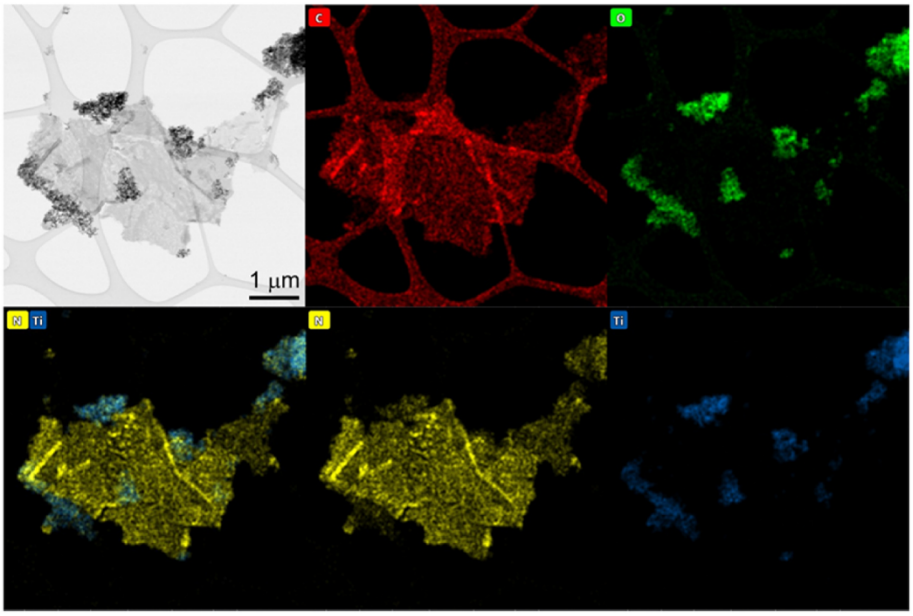

Fig. 6. EDS mapping scan of TiO_2+g-C_3N_4 coating from the recycled glass beads: C (red); O (green); N (golden) and Ti (blue). The sample was separated from beads by scratching the surface. (For interpretation of the references to colour in this figure legend, the reader is referred to the Web version of this article.)

with several high contrast lines in N mapping which was probably where the sheet was folded. This is typically seen in graphitic layer structures such as graphene. C and N mapping overlapped very well, thus verifying the composition of g-C_3N_4 (Fig. 6.). Ti and O distribution provided a clear view that the TiO_2 nanoparticles formed clusters and immobilized onto the g-C_3N_4 sheet, thus confirming the observations made under SEM examination. Fig. S8 displays the TEM image of the interface between TiO_2 and g-C_3N_4, which shows defects in the g-C_3N_4 sheets where TiO_2 nanoparticles are located. Considering the weight loss of the g-C_3N_4 layer that occurred during the TiO_2 coating, it is probable that the further coating of TiO_2 nano-powder damaged the previously applied g-C_3N_4 coating. Since the heat treatment was carried out at 500 °C for only 1 h, the effect on g-C_3N_4 structure was not marked. A longer isothermal run (5 h and 10 h) at 500 °C was assessed. The colour of the coated beads changed initially from yellow to grey and finally to white, which indicated that the g-C_3N_4 was burned off. It is worth noting here the g-C_3N_4 coated beads could survive calcination at 500 °C for 10 h in the absence of TiO_2 nanoparticles. This indicated that the TiO_2 nanoparticles accelerated the decomposition of the polymer.

3.3. Stability of catalyst coated beads to assess potential for continual use

The beads from the sunlight photocatalysis investigation in Brazil were evaluated for their suitability for re-use and compared to pristine catalyst coated beads using dye photodegradation. Rhodamine B degradation was tested with pristine and used g-C_3N_4 and TiO_2+g-C_3N_4 beads under UV–vis light irradiation (Fig. 7). The TiO_2+g-C_3N_4 beads performed better than g-C_3N_4 beads, which showed that the remaining TiO_2 worked with g-C_3N_4 and enhanced the photocatalytic activity. Moreover, four more cycled test were carried out by repeating the Rhodamine B degradation which demonstrated that both g-C_3N_4 and TiO_2+g-C_3N_4 co-coated beads showed good stability (Fig. 7). This result confirmed our previous work on methyl orange photodegradation using g-C_3N_4 coated expanded glass beads (Hui et al., 2021). XRD of used TiO_2+g-C_3N_4 co-coated beads shows an unchanged g-C_3N_4 (002) peak compared to pristine ones, with a decreased intensity for the anatase (101) peak (Fig. S9), while the surface morphologies of used catalysts looked almost no difference from pristine coated beads (Fig. S10), this may be related to the rearrangement of TiO_2 nanoparticles on g-C_3N_4 surface.

4. Towards application of solar-driven application of catalyst-coated glass beads

The current proof-of-concept study has demonstrated that photocatalytic degradation of the common freshwater cyanotoxin, MC-LR was readily achieved with sunlight and simulated sunlight in the presence of g-C_3N_4 and TiO_2+g-C_3N_4 coated onto buoyant recycled glass beads. The immobilization of the catalyst onto the beads (2–4 mm) allows ease of deployment which overcomes the problem of catalyst-water separation and retains a significant surface area. TiO_2+g-C_3N_4 co-coated beads showed improved performance compared to g-C_3N_4, while both materials displayed a superior activity compared to TiO_2 coated beads. The effective removal of MC-LR has been demonstrated under the current study design, however, further targeted research is required to address the effect of deployment in natural water samples. While the use of natural fresh water in assessing catalyst effectiveness appears desirable at first glance, it is impossible to carry out a study using natural freshwater in a way that is comparable to other studies since no two natural waters are the same. In previous work we have found that the amount of humic substances, general dissolved organics and even iron can all interact with the UV catalysis (Pestana et al., 2020a). Since this was the first stage to developing a field treatment it was key to perform the work in a reproducible manor, hence the use of artificial fresh water which is standardized and allows inter-study comparisons. Notwithstanding the problems inherent in the use of natural water samples, the effects of natural organic matter on the removal of dissolved microcystins was explored previously (Pestana et al., 2020a) and we demonstrated that in complex water samples (waste stabilization pond water) photocatalytic efficiency was decreased but that along with the removal of microcystins organic matter was also removed (both the humic and the protein portions showed a decrease in molecule size and concentration). Further, in our recent work (Pestana et al., 2020b) with TiO_2-coated glass beads and UV-LED irradiation we have demonstrated that the cells of the cyanobacterium *Microcystis aeruginosa* and its associated microcystins can be completely removed by a very similar catalyst system. Thus, it is not anticipated that the proposed system utilizing solar irradiation would struggle to remove cyanobacterial cells *in situ* even in the presence of natural organic matter, however this will have to be determined experimentally in the future. The current proof-of-principle study has demonstrated the feasibility of using any of the three investigated catalyst (non-time critical applications can use TiO_2 while more time critical applications can apply C_3N_4 or TiO_2+g-C_3N_4). These floating sunlight-active photocatalyst appear to be a very promising material for in-reservoir water treatment and blue-green algae management without requiring significant investment in water treatment plant infrastructure upgrades.

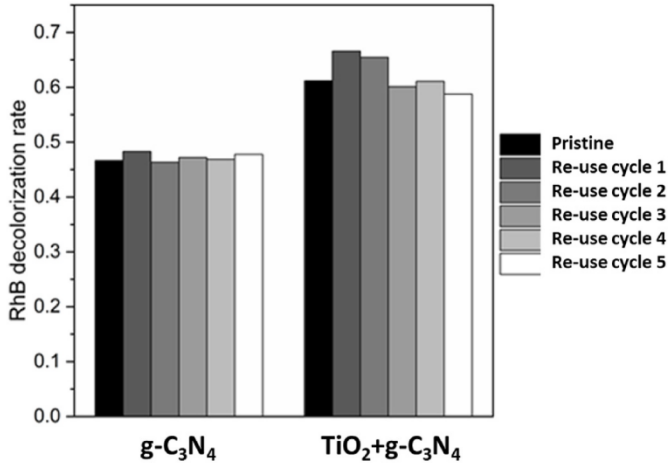

Fig. 7. Rhodamine B (RhB) degradation test using pristine and used samples: g-C_3N_4 (left); TiO_2+g-C_3N_4(right) over 5 test cycles.

CRediT author statement

Carlos J. Pestana Methodology, Investigation, Data Curation, Writing – Original Draft, Visualization, Jianing Hui. Investigation, Data Curation, Writing – Original Draft, Visualization, Formal Analysis, Dolores Camacho-Muñoz. Investigation, Data Curation, Writing – Review & Editing, Visualization, Christine Edwards. Resources, Writing – Review & Editing, Peter K. J. Robertson. Funding Acquisition, Writing – Review & Editing, John T. S. Irvine Funding Acquisition, Supervision, Writing – Review & Editing, Resources, Linda A. Lawton Conceptualisation, Funding Acquisition, Methodology, Project Administration, Supervision, Writing – Review & Editing.

Declaration of competing interest

The authors declare that they have no known competing financial interests or personal relationships that could have appeared to influence the work reported in this paper.

Data availability

Data will be made available on request.

Acknowledgements

We acknowledge the funding provided by the Engineering and Physical Sciences Research Council, UK (Global Challenge Research Fund: EP/P029280/1) towards carrying out this research. We also thank the support on electron microscopes from EPSRC Capital for Great Technologies (Grant EP/LP017008/1 and EP/R02375/1). J. Hui and C. Pestana would like to thank Professor José Capelo-Neto and Dr Nathan Skillen for their help with the experiments in Brazil.

Appendix A. Supplementary data

Supplementary data to this article can be found online at https://doi.org/10.1016/j.chemosphere.2022.136828.

References

Akkanen, J., Kukkonen, J.V.K., 2003. Biotransformation and bioconcentration of pyrene in Daphnia magna. Aquat. Toxicol. 64, 53–61. https://doi.org/10.1016/S0166-445X(03)00023-7.

Andersen, J., Han, C., O'Shea, K., Dionysiou, D.D., 2014. Revealing the degradation intermediates and pathways of visible light-induced NF-TiO2 photocatalysis of microcystin-LR. Appl. Catal. B Environ. https://doi.org/10.1016/j.apcatb.2014.02.025.

Camacho-Muñoz, D., Fervers, A.S., Pestana, C.J., Edwards, C., Lawton, L.A., 2020. Degradation of microcystin-LR and cylindrospermopsin by continuous flow UV-A photocatalysis over immobilised TiO2. J. Environ. Manag. 276 https://doi.org/10.1016/j.jenvman.2020.111368.

Chow, C.W.K., Drikas, M., House, J., Burch, M.D., Velzeboer, R.M.A., 1999. The impact of conventional water treatment processes on cells of the cyanobacterium Microcystis aeruginosa. Water Res. 33, 3253–3262. https://doi.org/10.1016/S0043-1354(99)00051-2.

Criado, M., Fernández-Jiménez, A., Palomo, A., 2007. Alkali activation of fly ash: effect of the SiO2/Na2O ratio. Part I: FTIR study. Microporous Mesoporous Mater. https://doi.org/10.1016/j.micromeso.2007.02.055.

Cui, Y., Zhengxin, D., Liu, P., Antonietti, M., Fu, Z., Wang, X., 2012. Metal free activation of H2O2 by g-C3N4 under visible light irradiation for the degradation of organic pollutants. Phys. Chem. Chem. Phys. 14, 1455–1462.

Edwards, C., Lawton, L.A., Coyle, S.M., Ross, P., 1996. Automated purification of microcystins. J. Chromatogr. A 734, 175–182.

Fan, G., Lin, X., You, Y., Du, B., Li, X., Luo, J., 2022. Magnetically separable ZnFe2O4/Ag3PO4/g-C3N4 photocatalyst for inactivation of Microcystis aeruginosa: characterization, performance and mechanism. J. Hazard Mater. 421, 126703 https://doi.org/10.1016/J.JHAZMAT.2021.126703.

Fan, G., You, Y., Wang, B., Wu, S., Zhang, Z., Zheng, X., Bao, M., Zhan, J., 2019. Inactivation of harmful cyanobacteria by Ag/AgCl@ZIF-8 coating under visible light: efficiency and its mechanisms. Appl. Catal. B Environ. 256 https://doi.org/10.1016/j.apcatb.2019.117866.

Fotiou, T., Triantis, T.M., Kaloudis, T., Pastrana-Martinez, L.M., Likodimos, V., Falaras, P., Silva, A.M.T., Hiskia, A., 2013. Photocatalytic degradation of microcystin-LR and off-odor compounds in water under UV-A and solar light with a nanostructured photocatalyst based on reduced graphene oxide-TiO2 composite. Identification of intermediate products. Ind. Eng. Chem. Res. 52, 13991–14000.

Gunaratne, H.Q.N., Pestana, C.J., Skillen, N., Hui, J., Saravanan, S., Edwards, C., Irvine, J.T.S., Robertson, P.K.J., Lawton, L.A., 2020. 'All in one' photo-reactor pod containing TiO 2 coated glass beads and LEDs for continuous photocatalytic destruction of cyanotoxins in water. Environ. Sci. Water Res. Technol. 6, 945–950. https://doi.org/10.1039/c9ew00711c.

He, X., Wang, A., Wu, P., Tang, S., Zhang, Y., Li, L., Ding, P., 2020. Photocatalytic degradation of microcystin-LR by modified TiO2 photocatalysis: a review. Sci. Total Environ. https://doi.org/10.1016/j.scitotenv.2020.140694.

Hui, J., Pestana, C.J., Caux, M., Gunaratne, H.Q.N., Edwards, C., Robertson, P.K.J., Lawton, L.A., Irvine, J.T.S., 2021. Graphitic-C3N4 coated floating glass beads for photocatalytic destruction of synthetic and natural organic compounds in water under UV light. J. Photochem. Photobiol. Chem. 405, 112935 https://doi.org/10.1016/j.jphotochem.2020.112935.

Humpage, A.R., Cunliffe, D., 2021. Exposure to cyanotoxins: understanding it and short-term interventions to prevent it - drinking Water. In: Chorus, I., Welker, M. (Eds.), Toxic Cyanobacteria in Water - A Guide to Their Public Health Consequences, Monitoring and Management. CRC Press, Oxon, pp. 305–333.

Kang, Y., Yang, Y., Yin, L.-Ch., Kang, X., Liu, G., Cheng, H.-M., 2015. A amorphous carbon nitride photocatalyst with greatly extended visible-light-responsive range for photocatalytic hydrogen generation. Adv. Mater. 27, 4573–4577.

Lawton, L.A., McElhiney, J., Edwards, C., 1999. Purification of closely eluting hydrophobic microcystins (peptide cyanotoxins) by normal-phase and reversed-phase flash chromatography. J. Chromatogr. A 848, 515–522. https://doi.org/10.1016/S0021-9673(99)00462-8.

Lawton, L.A., Robertson, P.K.J., Cornish, B.J.P.A., Marr, I.L., Jaspars, M., 2003. Processes influencing surface interaction and photocatalytic destruction of microcystins on titanium dioxide photocatalysts. J. Catal. 213, 109–113. https://doi.org/10.1016/S0021-9517(02)00049-0.

León, C., Boix, C., Beltrán, E., Peñuela, G., López, F., Sancho, J.V., Hernández, F., 2019. Study of cyanotoxin degradation and evaluation of their transformation products in surface waters by LC-QTOF MS. Chemosphere 229, 538–548. https://doi.org/10.1016/j.chemosphere.2019.04.219.

Li, Y., Lv, K., Ho, W., Dong, F., Wu, X., Xia, Y., 2017. Hybridization of rutile TiO2 (rTiO2) with g-C3N4 quantum dots (CN QDs): an efficient visible-light-driven Z-scheme hybridized photocatalyst. Appl. Catal. B Environ. 202, 611–619. https://doi.org/10.1016/j.apcatb.2016.09.055.

Liu, I., Lawton, L.A., Robertson, P.K.J., 2003. Mechanistic studies of the photocatalytic oxidation of microcystin-LR: an investigation of byproducts of the decomposition process. Environ. Sci. Technol. 37, 3214–3219. https://doi.org/10.1021/es0201855.

Ma, J., Wang, C., He, H., 2016. Enhanced photocatalytic oxidation of NO over g-C3N4-TiO2 under UV and visible light. Appl. Catal. B Environ. https://doi.org/10.1016/j.apcatb.2015.11.013.

Matthijs, H.C.P., Visser, P.M., Reeze, B., Meeuse, J., Slot, P.C., Wijn, G., Talens, R., Huisman, J., 2012. Selective suppression of harmful cyanobacteria in an entire lake with hydrogen peroxide. Water Res. 46, 1460–1472. https://doi.org/10.1016/j.watres.2011.11.016.

Menezes, I., Capelo-Neto, J., Pestana, C.J., Clemente, A., Hui, J., Irvine, J.T.S., Nimal Gunaratne, H.Q., Robertson, P.K.J., Edwards, C., Gillanders, R.N., Turnbull, G.A., Lawton, L.A., 2021. Comparison of UV-A photolytic and UV/TiO2 photocatalytic effects on Microcystis aeruginosa PCC7813 and four microcystin analogues: a pilot scale study. J. Environ. Manag. 298, 113519 https://doi.org/10.1016/j.jenvman.2021.113519.

Nawaz, M., Moztahida, M., Kim, J., Shahzad, A., Jang, J., Miran, W., Lee, D.S., 2018. Photodegradation of microcystin-LR using graphene-TiO2 sodium alginate aerogels. Carbohydr. Polym. 199, 109–118.

Nikokavoura, A., Trapalis, C., 2018. Graphene and g-C3N4 based photocatalysts for NOx removal A review. Appl. Surf. Sci. 430, 18–52.

Paerl, H.W., Huisman, J., 2008. Climate: blooms like it hot. Science (80- 320, 57–58. https://doi.org/10.1126/science.1155398.

Pestana, C.J., Edwards, C., Prabhu, R., Robertson, P.K.J., Lawton, L.A., 2015. Photocatalytic degradation of eleven microcystin variants and nodularin by TiO2 coated glass microspheres. J. Hazard Mater. 300, 347–353. https://doi.org/10.1016/j.jhazmat.2015.07.016.

Pestana, C.J., Hobson, P., Robertson, P.K.J., Lawton, L.A., Newcombe, G., 2020a. Removal of microcystins from a waste stabilisation lagoon: evaluation of a packed-bed continuous flow TiO2 reactor. Chemosphere 245, 125575. https://doi.org/10.1016/j.chemosphere.2019.125575.

Pestana, C.J., Portela Noronha, J., Hui, J., Edwards, C., Gunaratne, H.Q.N., Irvine, J.T.S., Robertson, P.K.J., Capelo-Neto, J., Lawton, L.A., 2020b. Photocatalytic removal of the cyanobacterium Microcystis aeruginosa PCC7813 and four microcystins by TiO2 coated porous glass beads with UV-LED irradiation. Sci. Total Environ. 745, 141154 https://doi.org/10.1016/j.scitotenv.2020.141154.

Porfirio, A.C.S., De Souza, J.L., Lyra, G.B., Maringolo Lemes, M.A., 2012. An assessment of the global UV solar radiation under various sky conditions in Maceió-Northeastern Brazil. Energy. https://doi.org/10.1016/j.energy.2012.05.042.

Rodríguez, E., Majado, M.E., Meriluoto, J., Acero, J.L., 2007a. Oxidation of microcystins by permanganate: reaction kinetics and implications for water treatment. Water Res. https://doi.org/10.1016/j.watres.2006.10.004.

Rodríguez, E., Onstad, G.D., Kull, T.P.J., Metcalf, J.S., Acero, J.L., von Gunten, U., 2007b. Oxidative elimination of cyanotoxins: comparison of ozone, chlorine, chlorine dioxide and permanganate. Water Res. https://doi.org/10.1016/j.watres.2007.03.033.

Santos, A.A., Guedes, D.O., Barros, M.U.G., Oliveira, S., Pacheco, A.B.F., Azevedo, S.M.F.O., Magalhães, V.F., Pestana, C.J., Edwards, C., Lawton, L.A., Capelo-Neto, J., 2021. Effect of hydrogen peroxide on natural phytoplankton and bacterioplankton in a drinking water reservoir: mesocosm-scale study. Water Res. 197, 117069 https://doi.org/10.1016/j.watres.2021.117069.

Song, J., Wang, Xuejiang, Ma, J., Wang, Xin, Wang, J., Xia, S., 2018a. Removal of Microsystis aeruginosa and Microcystin LR using a graphitic C3N4 TiO2 floating photocatalyst under visible light irradiation. Chem. Eng. J. 348, 380–388.

Song, J., Wang, Xuejiang, Ma, J., Wang, Xin, Wang, J., Xia, S., Zhao, J., 2018b. Removal of Microcystis aeruginosa and Microcystin-LR using a graphitic-C3N4/TiO2 floating photocatalyst under visible light irradiation. Chem. Eng. J. 348, 380–388. https://doi.org/10.1016/J.CEJ.2018.04.182.

Song, J., Wang, Xuejiang, Ma, J., Wang, Xin, Wang, J., Zhao, J., 2018c. Visible-light-driven in situ inactivation of Microcystis aeruginosa with the use of floating g-C3N4 heterojunction photocatalyst_ Performance, mechanisms and implications. Appl. Catal. B Environ. 226, 83–92.

Su, Y., Deng, Y., Du, Y., 2013. Alternative pathways for photocatalytic degradation of microcystin-LR revealed by TiO2 nanotubes. J. Mol. Catal. Chem. https://doi.org/10.1016/j.molcata.2013.02.031.

Turner, A.D., Waack, J., Lewis, A., Edwards, C., Lawton, L.A., 2018. Development and single-laboratory validation of UHPLC-MS/MS method for quantitation of microcystins and nodularin in natural water, cyanobacteria, shellfish and algal supplement tablet powders. J. Chromatogr. B 1074–1075, 111–123.

Wang, Xin, Wang, Xuejiang, Zhao, J., Song, J., Su, C., Wang, Z., 2018. Surface modified TiO2 floating photocatalyst with PDDA for efficient adsorption and photocatalytic inactivation of Microcystis aeruginosa. Water Res. https://doi.org/10.1016/j.watres.2017.12.062.

Wang, Xin, Wang, Xuejiang, Zhao, J., Song, J., Wang, J., Ma, R., Ma, J., 2017a. Solar light-driven photocatalytic destruction of cyanobacteria by F-Ce-TiO2/expanded perlite floating composites. Chem. Eng. J. 320, 253–263. https://doi.org/10.1016/j.cej.2017.03.062.

Wang, Xin, Wang, Xuejiang, Zhao, J., Song, J., Zhou, L., Wang, J., Tong, X., Chen, Y., 2017b. An alternative to in situ photocatalytic degradation of microcystin-LR by worm-like N, P co-doped TiO2/expanded graphite by carbon layer (NPT-EGC) floating composites. Appl. Catal. B Environ. https://doi.org/10.1016/j.apcatb.2017.01.046.

WHO, W.H.O., 2020. Cyanobacterial Toxins : Microcystins. Background document for drinking-water quality and Guidelines for safe recreational water environments, Geneva.

Xing, Z., Zhang, J., Cui, J., Yin, J., Zhao, T., Kuang, J., Xiu, Z., Wan, N., Zhou, W., 2018. Recent advances in floating TiO2 based photocatalysts for environmental application. Appl. Catal. B Environ. 225, 452–467.

Zhang, Y., Thomas, A., Antonietti, M., Wang, X., 2009. Activation of carbon nitride solids by protonation: morphology changes, enhanced ionic conductivity, and photoconduction experiments. J. Am. Chem. Soc. https://doi.org/10.1021/ja808329f.

Supporting Information for:

Solar-driven semi-conductor photocatalytic water treatment (TiO_2, g-C_3N_4, and TiO_2+g-C_3N_4) of cyanotoxins: proof-of-concept study with microcystin-LR

Carlos J. Pestana [a‡*], Jianing Hui [b‡], Dolores Camacho-Muñoz [a], Christine Edwards [a], Peter K. J. Robertson [c], John T. S. Irvine [b], Linda A. Lawton [a]

[a] School of Pharmacy and Life Sciences, Robert Gordon University, Garthdee Road, Aberdeen, Scotland, AB10 7GJ, UK.

[b] School of Chemistry, University of St Andrews, North Haugh, St Andrews, Scotland, KY16 9ST, UK.

[c] School of Chemistry and Chemical Engineering, the Queen's University of Belfast, Stanmillis Road, Belfast, Northern Ireland, BT9 5AG, UK.

‡ These authors contributed equally.

Figure S1

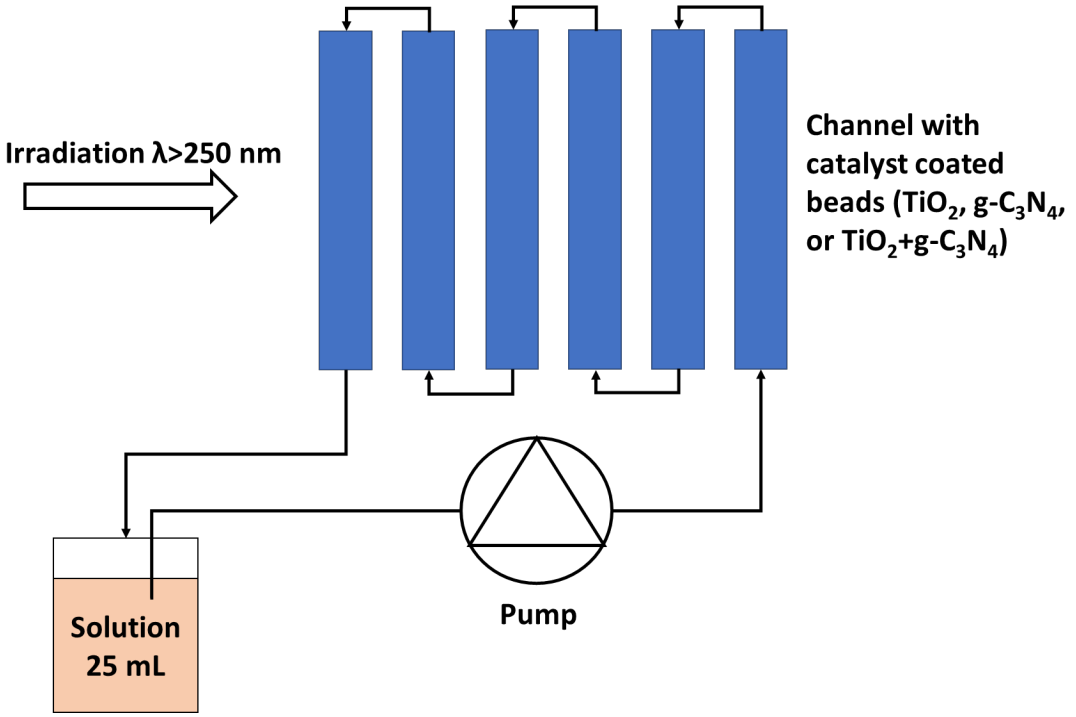

Fig. S1. Schematic representation of six-channel photoreactor used for dye-degradation experiments to determine stability of the catalyst coated glass beads (either TiO_2, g-C_3N_4, or TiO_2+g-C_3N_4).

Figure S2

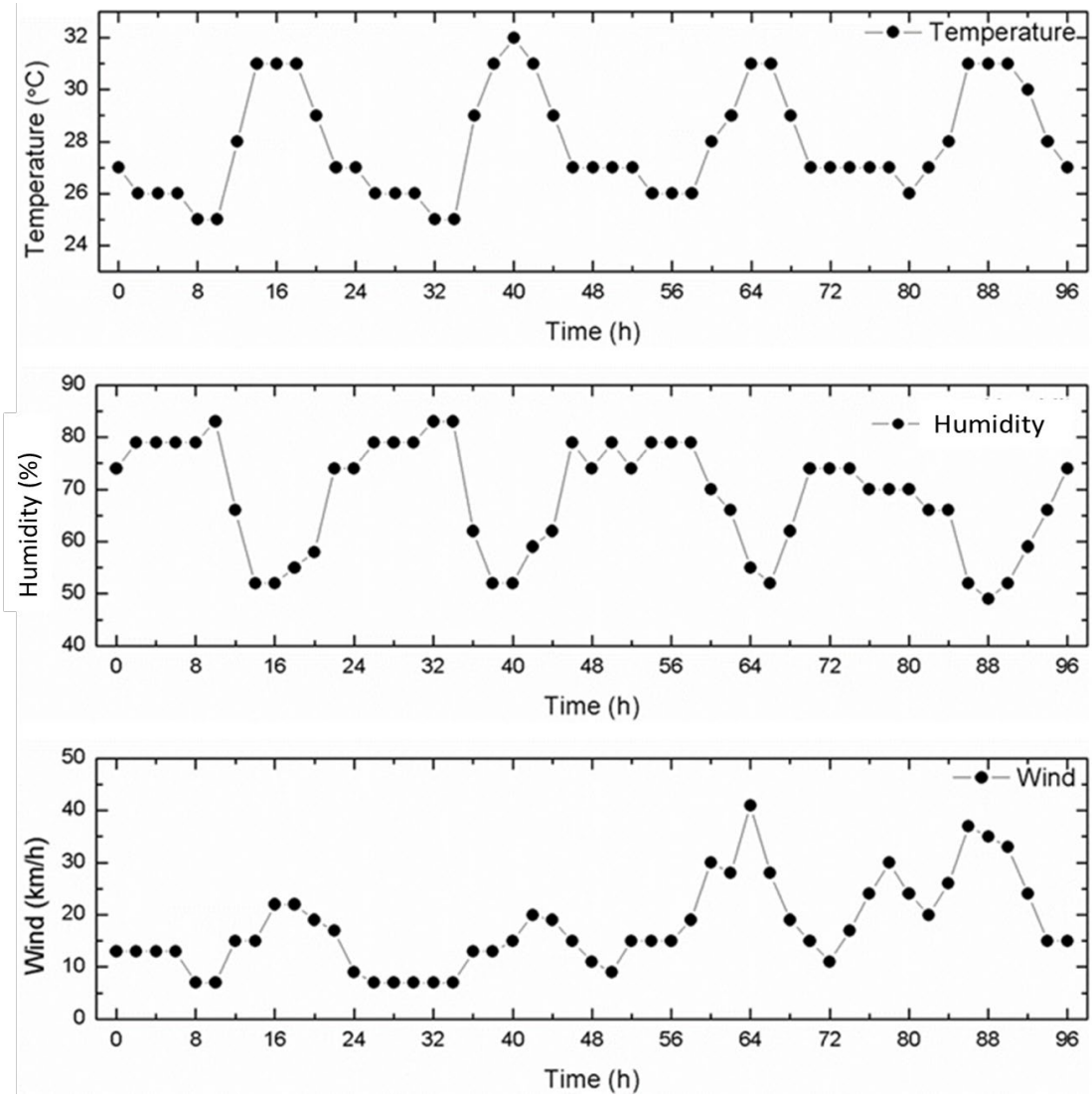

Fig. S2. Additional climatic information for conditions during the solar degradation study conducted in Fortaleza, Brazil in October 2019. Temperature, humidity and windspeeds are presented for the 96 h duration of the experiment.

Figure S3

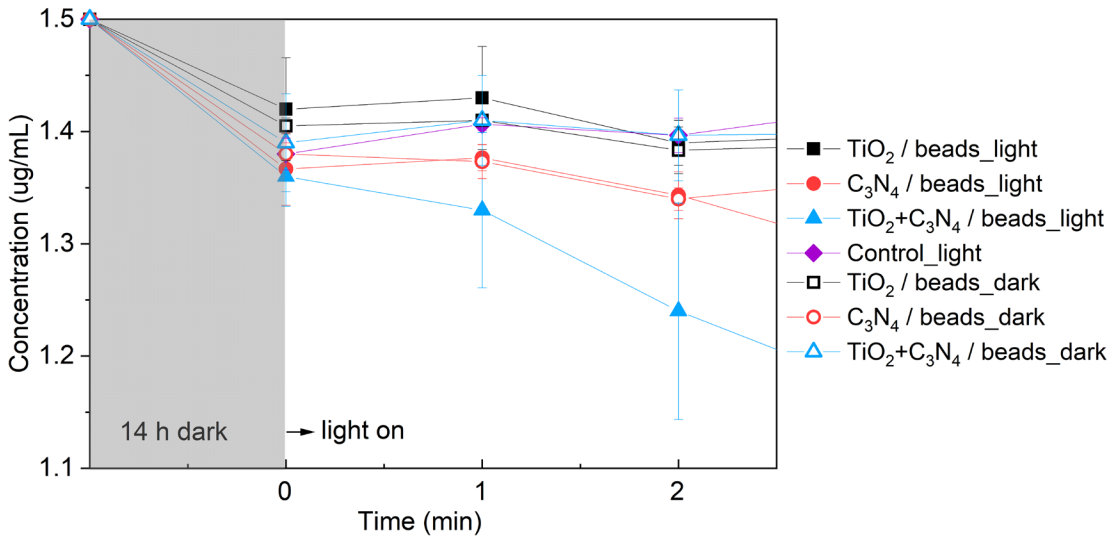

Fig. S3. Photocatalytic destruction of MC-LR under simulated sunlight irradiation: Zoomed in section of the initial degradation over the first two minutes. Initial toxin concentration is 1.5 µg mL^{-1}. (n = 3, Error = 1SD)

Figure S4

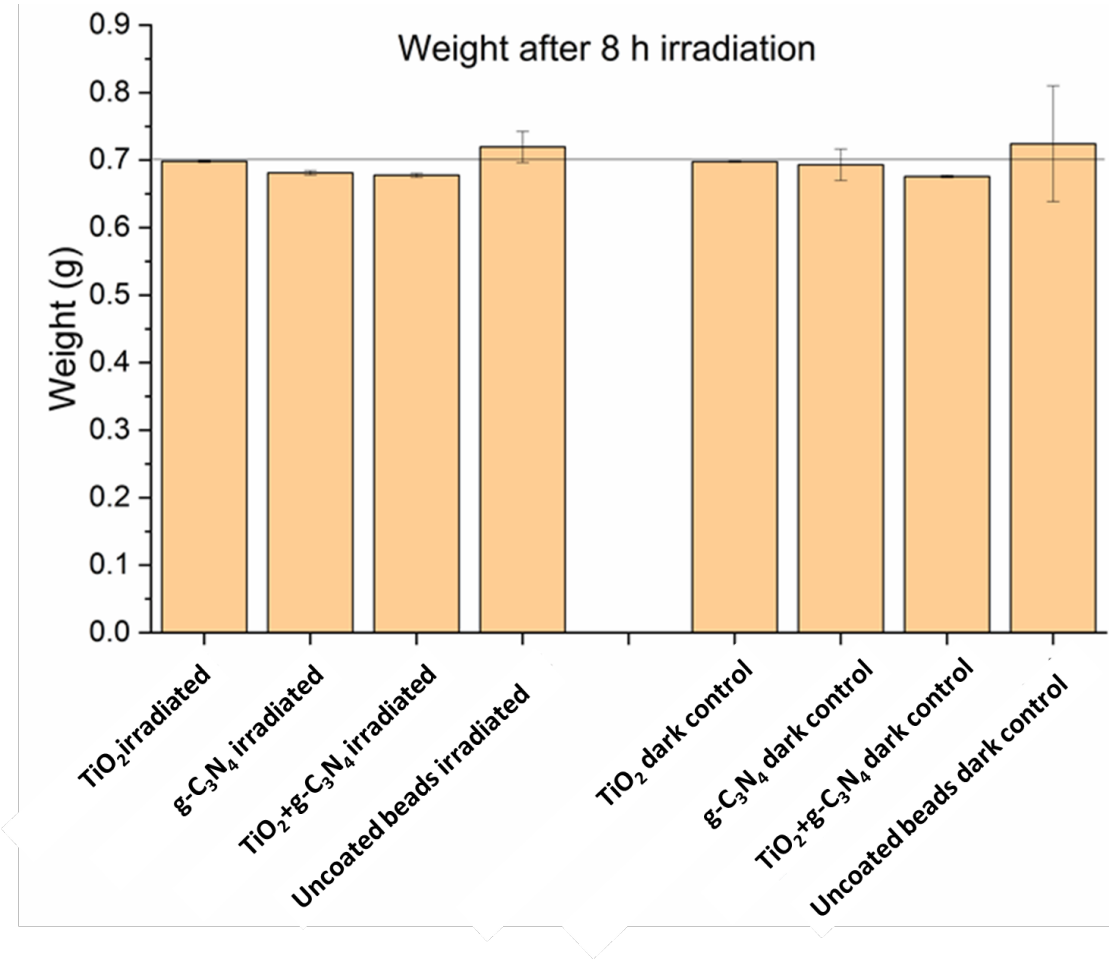

Fig. S4. Weight of catalyst after 8 h of irradiation, measured to confirm stability of the coating on the beads made from recycled glass. Theoretical initial mass of catalyst 700 mg based on 10% (w/w) catalyst load on the beads. (n=3, error = 1SD).

Figure S5

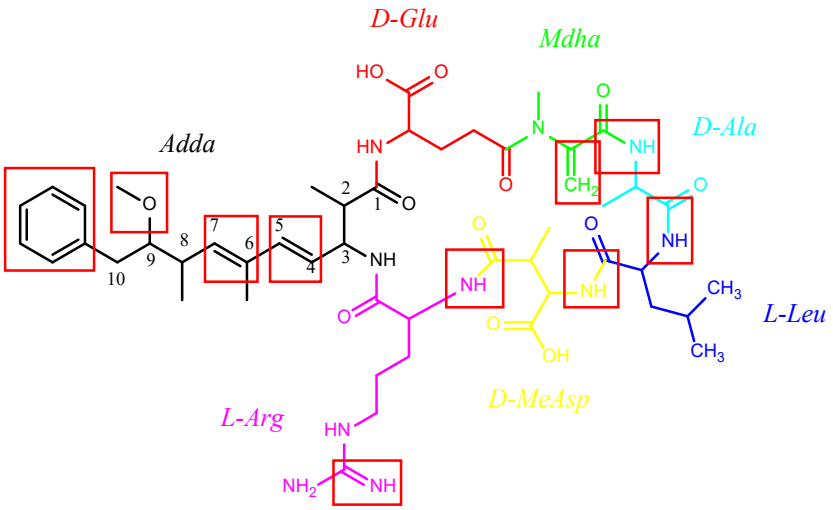

Fig. S5. The molecular structure of MC-LR with the possible attack positions highlighted by red square (adapted from He et al., 2020).

Table S1

Table S1. Product ions of the different proposed degradation pathways of MC-LR under simulated solar irradiation over three different photocatalysts (TiO_2, g-C_3N_4, TiO_2+g-C_3N_4) with yellow: initial attack on the benzene ring and methoxy group of the Adda chain; red: initial attack on C6-C7 double bond.

m/z	Rt (min)	TiO_2	g-C_3N_4	TiO_2+g-C_3N_4
1045.5360	3.59	x		x
1029.5601	2.69-3.22	x	x	x
1027.5664	2.77-3.25		x	x
1025.5310	3.67	x	x	x
1011.5482	2.76-3.55	x	x	x
1009.5331	3.15-3.56	x	x	x
965.5432	4.36	x		
965.5492	2.30		x	x
877.4780	2.69-3.23	x	x	x
877.4949	2.18		x	x
865.4406	1.35-1.43	x	x	x
835.4327	1.43-1.52	x	x	x
815.3893	1.33	x	x	x
745.4191	1.96	x	x	x
700.3647	2.81-3.15		x	
700.3650	2.81	x		
564.3589	1.61	x		
525.2879	1.52	x		
525.2677	1.52		x	x
515.2847	2.57-3.32	x	x	x
481.2624	1.43	x	x	x
437.2361	1.34, 1.52		x	x
437.2361	1.34	x		

Table S2

Table S2. Elemental quantification of uncoated beads using EDS. The detected Au is from gold coating for enhancing conductivity purpose.

Element	Weight %	Atomic %
O	48.40	61.98
Na	12.21	10.88
Mg	1.36	1.15
Al	1.70	1.29
Si	29.67	21.64
K	0.41	0.22
Ca	5.27	2.69
Fe	0.14	0.05
Au	0.84	0.09

Figure S6

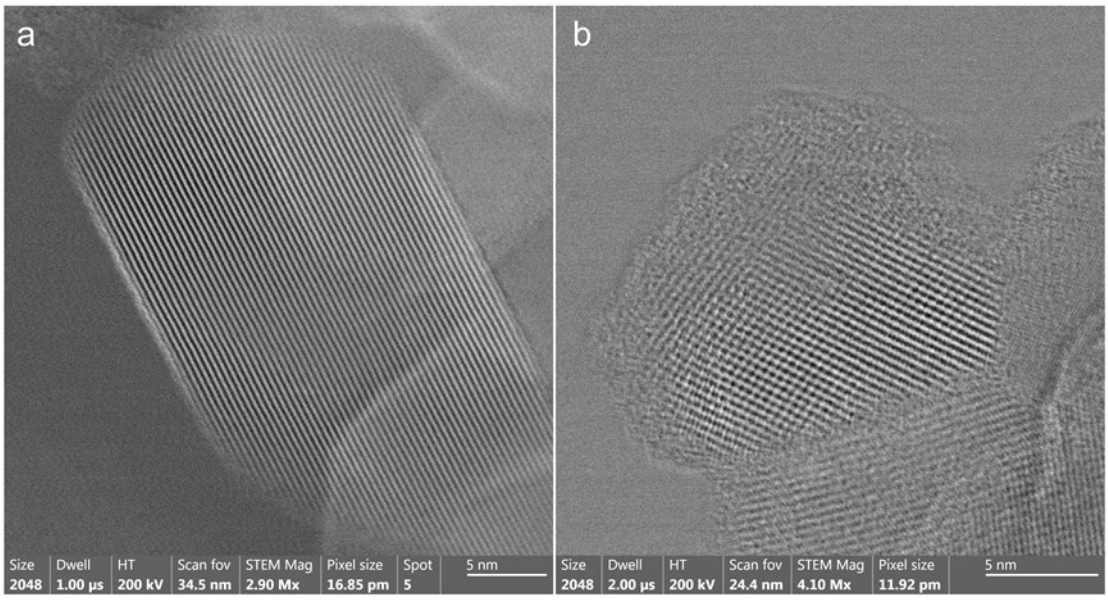

Fig. S6. High resolution TEM images of TiO_2/beads shedding material. Both particles are TiO_2 (anatase) nanoparticles.

Figure S7

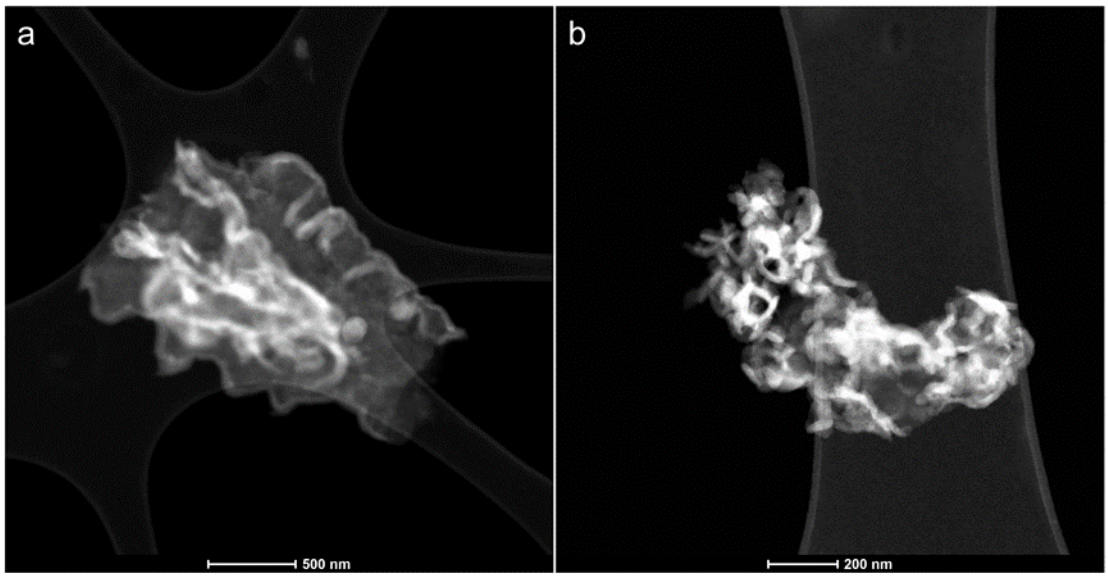

Fig. S7. High resolution TEM images of g-C_3N_4 bead scrappings. Both are g-C_3N_4 in different shape: (a) spread sheet with folds; (b) wrapped sheet.

Table S3

Table S3. Elemental quantification of coated glass beads.

	TiO_2		g-C_3N_4		TiO_2+g-C_3N_4	
Element	Weight (%)	Atomic (%)	Weight (%)	Atomic (%)	Weight (%)	Atomic (%)
C	6.55	11.25	24.33	30.81	21.12	29.84
N	0.00	0.00	28.43	30.87	12.13	14.70
O	49.52	63.92	30.93	29.41	38.01	40.32
Na	3.78	3.40	2.53	1.67	3.19	2.36
Mg	0.00	0.00	0.47	0.29	1.04	0.73
Al	0.91	0.70	0.41	0.23	0.72	0.45
Si	12.03	8.84	11.18	6.05	11.86	7.17
Ca	1.87	0.97	1.74	0.66	3.11	1.32
Ti	25.33	10.92	0.00	0.00	8.81	3.12
Totals	100.00	100.00	100.00	100.00	100.00	100.00

Figure S8

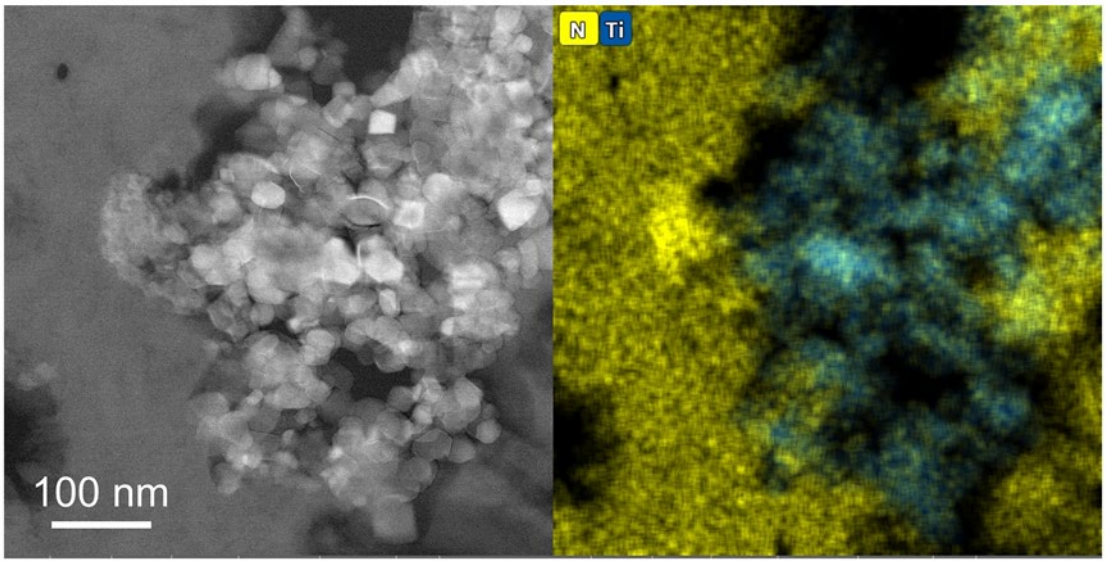

Fig. S8. TEM image (left) and EDS mapping (right) of TiO_2-C_3N_4 interface.

Figure S9

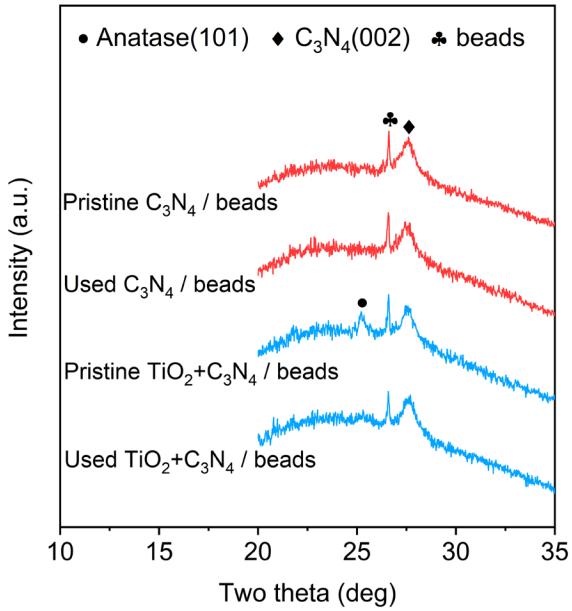

Fig. S9. Powder X-ray diffraction patterns of pristine coated beads and used beads. Red: C_3N_4 coated beads; blue: TiO_2+g-C_3N_4 co-coated beads.

Figure S10

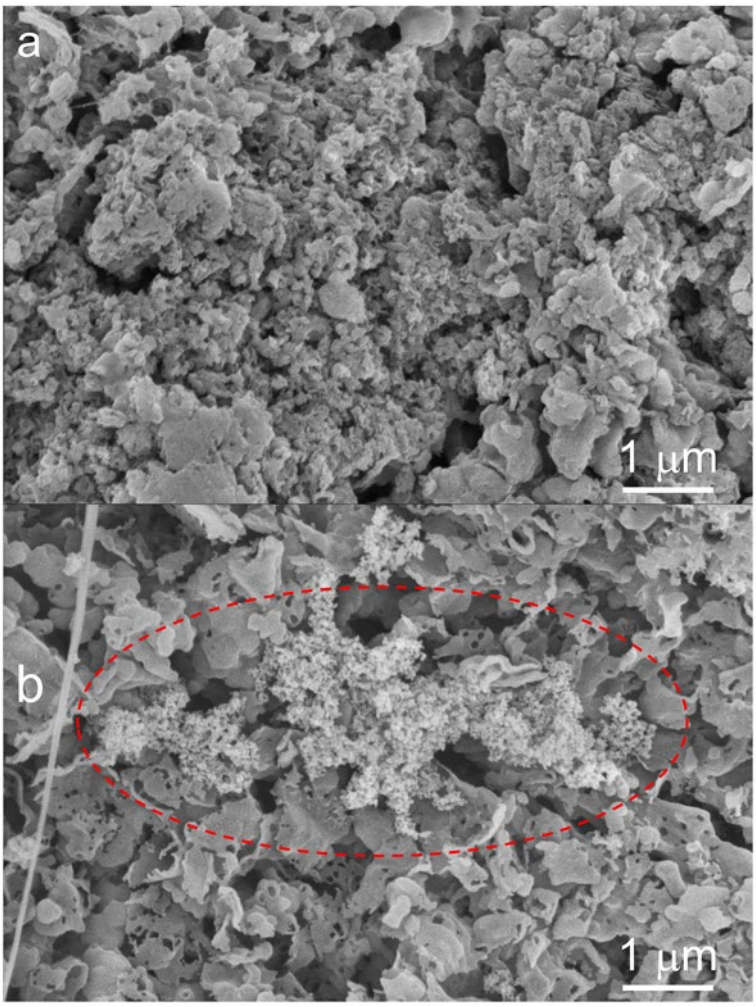

Fig. S10. SEM images of used g-C_3N_4 (a) and TiO_2+C_3N_4 (b) beads after 96 h solar irradiation test. TiO_2 nanoparticles immobilized on C_3N_4 surface have been highlighted with red dashed line.

References

He, X., Wang, A., Wu, P., Tang, S., Zhang, Y., Li, L., Ding, P., 2020. Photocatalytic degradation of microcystin-LR by modified TiO_2 photocatalysis: A review. Sci. Total Environ. 743, 140694. https://doi.org/10.1016/j.scitotenv.2020.140694